Sandwich-Type Silicotungstates: Structure and Magnetic Properties of the Dimeric Polyoxoanions [{SiM$_2$W$_9$O$_{34}$(H$_2$O)}$_2$]$^{12-}$ (M = Mn^{2+}, Cu^{2+}, Zn^{2+})

Ulrich Kortz,*,† Samih Isber,‡ Michael H. Dickman,§ and Didier Ravot‖

Department of Chemistry and Department of Physics, American University of Beirut, Bliss Street, P.O. Box 11-0236, Beirut, Lebanon, Department of Chemistry, Georgetown University, Box 571227, Washington, D.C. 20057-1227, and Laboratoire de Physico-Chimie de la Matière Condensée, Université Montpellier II, case courrier 003, 34095 Montpellier Cedex 5, France

The novel dimeric silicotungstates [{SiM$_2$W$_9$O$_{34}$(H$_2$O)}$_2$]$^{12-}$ (M = Mn^{2+}, Cu^{2+}, Zn^{2+}) have been synthesized and characterized by IR spectroscopy, elemental analysis, and magnetic measurements. X-ray single-crystal analyses were carried out on K$_4$Na$_6$Mn[{SiMn$_2$W$_9$O$_{34}$(H$_2$O)}$_2$]·33H$_2$O (**1**), which crystallizes in the triclinic system, space group $P\bar{1}$, with $a = 12.2376(7)$ Å, $b = 13.6764(8)$ Å, $c = 15.6177(9)$ Å, $\alpha = 70.2860(10)°$, $\beta = 79.9150(10)°$, $\gamma = 70.2760(10)°$, and $Z = 1$; K$_3$Na$_5$[{SiCu$_2$W$_9$O$_{34}$(H$_2$O)}$_2$]·26H$_2$O (**2**) crystallizes in the triclinic system, space group $P\bar{1}$, with $a = 11.4271(12)$ Å, $b = 12.5956(13)$ Å, $c = 15.3223(16)$ Å, $\alpha = 80.456(2)°$, $\beta = 76.383(2)°$, $\gamma = 76.968(2)°$, and $Z = 1$; K$_4$Na$_6$[{SiZn$_2$W$_9$O$_{34}$(H$_2$O)}$_2$]·34H$_2$O (**3**) crystallizes also in the triclinic system, space group $P\bar{1}$, with $a = 12.2596(14)$ Å, $b = 13.2555(15)$ Å, $c = 16.2892(18)$ Å, $\alpha = 96.431(2)°$, $\beta = 100.944(2)°$, $\gamma = 110.404(2)°$, and $Z = 1$. The polyanions consist of two lacunary B-α-[SiW$_9$O$_{34}$]$^{10-}$ Keggin moieties linked via a rhomblike M$_4$O$_{16}$ (M = Mn, Cu, Zn) group leading to a sandwich-type structure. Magnetic measurements show that the central Mn$_4$ unit in **1** exhibits antiferromagnetic ($J = -1.77(5)$ cm^{-1}) as well as weak ferromagnetic ($J' = 0.08(2)$ cm^{-1}) Mn−Mn exchange interactions. In **2** the Cu−Cu exchange interactions are antiferromagnetic ($J = -0.10(2)$ cm^{-1}, $J' = -0.29(2)$ cm^{-1}).

Introduction

Polyoxometalates constitute a unique class of inorganic compounds due to the structural variety as well as interesting and often unexpected properties in fields as diverse as catalysis, medicine, and magnetochemistry.[1−4] At the same time it must be pointed out that the mechanism of formation of polyoxometalates is not well understood and commonly described as self-assembly. Nevertheless the synthesis of polyoxometalates is mostly rather simple and straightforward, once the proper reaction conditions have been identified.

Transition metal substituted polyoxometalates can also be of interest for their magnetic properties. Structures that contain more than one paramagnetic transition metal ion in close proximity may exhibit exchange-coupled spins leading to large spin ground states, one of the goals in molecular magnetism.[5,6] The polyoxometalate matrix may be considered a diamagnetic host encapsulating and thereby isolating magnetic clusters of transition metals.

Lacunary polyoxometalates are usually synthesized from complete precursor ions by loss of one or more MO$_6$ octahedra. Reaction of a stable, lacunary polyoxometalate with transition metal ions usually leads to a product with the heteropolyanion framework unchanged. Depending upon the coordination requirement and the size of a given transition metal ion, the geometry of the reaction product can therefore often be predicted.

Trying to understand the interaction of metastable, lacunary polyoxoanions (e.g., [γ-SiW$_{10}$O$_{36}$]$^{8-}$) with transition metal ions represents more of a challenge, because dissolution of the lacunary polyanion in water initiates isomerization. The behavior of silicotungstates in aqueous solution has been extensively studied by Tézé et al. and is quite well understood.[7] The interaction of γ-decatungstosilicate, [γ-SiW$_{10}$O$_{36}$]$^{8-}$, with several metal ions has recently been studied, and reaction with Cr^{3+}, Mn$^{2+,3+}$, Fe^{3+}, and VO$_3^-$ ions led to disubstituted, monomeric γ-Keggin ions.[8a−d] However, reaction with phenyltin trichloride (C$_6$H$_5$SnCl$_3$) resulted in a dimeric species where two phenyltin groups link two γ-decatungstosilicate ions.[9] Kortz et al. have shown recently that insertion of Ni^{2+} ions into [γ-SiW$_{10}$O$_{36}$]$^{8-}$ in aqueous solution initiates isomerization and dimerization leading to a polyoxoanion composed of two di-nickel-substituted

---

* Author to whom correspondence should be addressed. E-mail: ulrich. kortz@aub.edu.lb. Fax: +961 1 744461.
† Department of Chemistry, American University of Beirut.
‡ Department of Physics, American University of Beirut.
§ Georgetown University.
‖ Université Montpellier II.

(1) Hill, C. L., Ed. *Chem. Rev.* Polyoxometalates, **1998**, *98*.
(2) *Polyoxometalates: from Platonic Solids to Anti-Retroviral Activity*; Pope, M. T., Müller, A., Eds.; Kluwer: Dordrecht, The Netherlands, 1994.
(3) Pope, M. T.; Müller, A. *Angew. Chem., Int. Ed. Engl.* **1991**, *30*, 34−48.
(4) Pope, M. T. *Heteropoly and Isopoly Oxometalates*; Springer-Verlag: Berlin, 1983.
(5) Gatteschi, D. *Adv. Mater.* **1994**, *6*, 635.
(6) *Magnetic Molecular Materials*; Gatteschi, D., Kahn, O., Miller, J. S., Palacio, F., Eds.; Kluwer: Dordrecht, The Netherlands, 1991.

(7) Tézé, A.; Hervé, G. *Inorganic Syntheses*; John Wiley & Sons: New York, 1990; Vol. 27, p 85.
(8) (a) Wassermann, K.; Lunk, H.-J.; Palm, R.; Fuchs, J.; Steinfeldt, N.; Stösser, R.; Pope, M. T. *Inorg. Chem.* **1996**, *35*, 3273. (b) Zhang, X.-Y.; O'Connor, C. J.; Jameson, G. B.; Pope, M. T. *Inorg. Chem.* **1996**, *35*, 30. (c) Mizuno, N.; Nozaki, C.; Kiyoto, I.; Misono, M. *J. Am. Chem. Soc.* **1998**, *120*, 9267. (d) Canny, J.; Thouvenot, R.; Tézé, A.; Hervé, G.; Leparulo-Loftus, M.; Pope, M. T. *Inorg. Chem.* **1991**, *30*, 976.
(9) Xin, F.; Pope, M. T. *Inorg. Chem.* **1996**, *35*, 5693.

Table 1. Crystal Data and Structure Refinement for $K_4Na_6Mn[\{SiMn_2W_9O_{34}(H_2O)\}_2]\cdot33H_2O$ (**1**), $K_3Na_5[\{SiCu_2W_9O_{34}(H_2O)\}_2]\cdot26H_2O$ (**2**), and $K_4Na_6[\{SiZn_2W_9O_{34}(H_2O)\}_2]\cdot34H_2O$ (**3**)

	1	2	3
empirical formula	$K_4Mn_5Na_6O_{103}Si_2W_{18}$	$Cu_4K_3Na_5O_{96}Si_2W_{18}$	$K_4Na_6O_{104}Si_2W_{18}Zn_4$
fw	5582.5	5387.9	5585.3
space group (No.)	$P\bar{1}$ (2)	$P\bar{1}$ (2)	$P\bar{1}$ (2)
a, Å	12.2376(7)	11.4271(12)	12.2596(14)
b, Å	13.6764(8)	12.5956(13)	13.2555(15)
c, Å	15.6177(9)	15.3223(16)	16.2892(18)
α, deg	70.2860(10)	80.456(2)	96.431(2)
β, deg	79.9150(10)	76.383(2)	100.944(2)
γ, deg	70.2760(10)	76.968(2)	110.404(2)
vol, Å^3	2310.8(2)	2073.3(4)	2389.8(5)
Z	1	1	1
temp, °C	-70	-70	-100
wavelength, Å	0.71073	0.71073	0.71073
density (calcd), g/cm^3	4.01	4.32	3.88
abs coeff, mm^{-1}	23.315	26.189	22.895
$R(F_o)^a$	0.041	0.057	0.053
$R_w(F_o)^b$	0.097	0.129	0.135

^{a} $R = \sum||F_o| - |F_c||/\sum|F_o|$. ^{b} $R_w = [\sum w(F_o^2 - F_c^2)^2/\sum w(F_o^2)^2]^{1/2}$.

β-Keggin units, $[\{\beta\text{-}SiNi_2W_{10}O_{36}(OH)_2(H_2O)\}_2]$.[12-10] In order to find out if the same structure could be formed with other first-row transition metals we investigated the interaction of $[\gamma\text{-}SiW_{10}O_{36}]^{8-}$ with Mn^{2+}, Cu^{2+}, and Zn^{2+} in some detail.

Experimental Section

Synthesis. $K_8[\gamma\text{-}SiW_{10}O_{36}]\cdot12H_2O$ was prepared according to a published procedure by Tézé and Hervé and confirmed by infrared spectroscopy.[11] All other reagents were used as purchased without further purification.

$K_4Na_6Mn[\{SiMn_2W_9O_{34}(H_2O)\}_2]\cdot33H_2O$ (1). A 2.23 g (0.75 mmol) sample of $K_8[\gamma\text{-}SiW_{10}O_{36}]$ was added with stirring to a solution of 0.36 g (2.25 mmol) $MnCl_2\cdot2H_2O$ in 100 mL of a 1.0 M sodium acetate buffer (pH 4.8). This solution was heated to 90 °C for 40 min and then cooled to room temperature. Addition of solid KCl (10 g) led to a yellow product, which was filtered off and air-dried. Yield: 0.39 g (20%). Single crystals suitable for X-ray crystallography were obtained by slow evaporation of the above solution. IR: 984 (w), 948 (s), 904 (vs), 876 (vs), 849 (sh), 758 (vs), 720 (w), 535 (w), 509 (w), 485 (w) cm^{-1}. Anal. Calcd for $K_{3.4}Na_{7.2}Mn_{0.7}[\{SiMn_2W_9O_{34}(H_2O)\}_2]\cdot35H_2O$: K, 2.34; Na, 2.92; W, 58.29; Mn, 4.55; Si, 0.99. Found: K, 2.29; Na, 2.87; W, 58.51; Mn, 4.56; Si, 0.63.

$K_3Na_5[\{SiCu_2W_9O_{34}(H_2O)\}_2]\cdot26H_2O$ (2). The synthetic procedure above was followed using 0.38 g (2.25 mmol) $CuCl_2\cdot2H_2O$ instead of $MnCl_2\cdot2H_2O$. Addition of solid KCl (10 g) to the solution led to a light-green product, which was filtered off and air-dried. Yield: 0.53 g (27%). Single crystals were obtained by slow evaporation of the above solution. IR: 986 (w), 949 (s), 899 (vs), 881 (vs), 849 (sh), 761 (vs), 724 (vs), 534 (w), 509 (w), 491 (w) cm^{-1}. Anal. Calcd for $K_4Na_8\text{-}[\{SiCu_2W_9O_{34}(H_2O)\}_2]\cdot23H_2O$: K, 2.84; Na, 3.34; W, 60.19; Cu, 4.62; Si, 1.02. Found: K, 3.07; Na, 3.38; W, 60.25; Cu, 4.60; Si, 0.62.

$K_4Na_6[\{SiZn_2W_9O_{34}(H_2O)\}_2]\cdot34H_2O$ (3). The procedure above was followed using 0.31 g (2.25 mmol) $ZnCl_2$. Addition of solid KCl (10 g) to the solution led to a white product, which was filtered off and air-dried. Yield: 0.31 g (16%). Single crystals were obtained by slow evaporation of the above solution. IR: 985 (w), 948 (s), 906 (vs), 895 (vs), 848 (sh), 757 (vs), 725 (vs), 538 (w), 513 (w), 493 (w) cm^{-1}. Anal. Calcd for $K_3Na_9[\{SiZn_2W_9O_{34}(H_2O)\}_2]\cdot34H_2O$: K, 2.06; Na, 3.64; W, 58.18; Zn, 4.60; Si, 0.99. Found: K, 2.00; Na, 3.66; W, 58.13; Zn, 4.37; Si, 1.10. All elemental analyses were performed by the Service Central d'Analyse of CNRS at 69390 Vernaison, France.

(10) Kortz, U.; Jeannin, Y. P.; Tézé, A.; Hervé, G.; Isber, S. *Inorg. Chem.* **1999**, *38*, 3670.

(11) Tézé, A.; Hervé, G. *Inorganic Syntheses*; John Wiley & Sons: New York, 1990; Vol. 27, p 88.

(12) Sheldrick, G. M. *SADABS*; Siemens Analytical X-ray Instrument Division: Madison, WI, 1995.

X-ray Crystallography. A yellow block of **1** with dimensions 0.10 × 0.16 × 0.24 mm^3 was mounted on a glass fiber for indexing and intensity data collection at 203 K on a Siemens SMART-CCD single-crystal diffractometer using Mo Kα radiation (λ = 0.71073 Å). Of the 11022 unique reflections ($2\theta_{max}$ = 56.68°), 9204 reflections (R_{int} = 0.051) were considered observed ($I > 2\sigma(I)$). Direct methods were used to solve the structure and to locate the tungsten atoms (SHELXS86). Then the remaining atoms were found from successive difference maps (SHELXL93). The final cycle of refinement, including the atomic coordinates, anisotropic thermal parameters (all metal atoms), and isotropic thermal parameters (silicon and oxygen atoms) converged at R = 0.041 and R_w = 0.097 ($I > 2\sigma(I)$). In the final difference map the deepest hole was -3.382 e Å^{-3} and the highest peak 2.372 e Å^{-3}.

A green column of **2** with dimensions 0.06 × 0.10 × 0.38 mm^3 was used for data collection at 203 K on a Siemens SMART-CCD diffractometer. Of the 9942 unique reflections ($2\theta_{max}$ = 56.92°), 6982 reflections (R_{int} = 0.087) were considered observed ($I > 2\sigma(I)$). The procedure followed for structure solution and refinement was analogous to that followed for **1**. The final cycle of refinement converged at R = 0.057 and R_w = 0.129 ($I > 2\sigma(I)$). In the final difference map the deepest hole was -4.246 e Å^{-3} and the highest peak 3.956 e Å^{-3}.

A colorless block of **3** with dimensions 0.10 × 0.32 × 0.48 mm^3 was used for data collection at 173 K on a Siemens SMART-CCD diffractometer. Of the 11377 unique reflections ($2\theta_{max}$ = 56.70°), 10156 reflections (R_{int} = 0.064) were considered observed ($I > 2\sigma(I)$). The procedure followed for structure solution and refinement was analogous to that followed for **1**. The final cycle of refinement converged at R = 0.053 and R_w = 0.135 ($I > 2\sigma(I)$). In the final difference map the deepest hole was -5.107 e Å^{-3} and the highest peak 4.255 e Å^{-3}.

Routine Lorentz and polarization corrections were applied to all structures, and an absorption correction was performed using the *SADABS* program.[12] Crystallographic data are summarized in Table 1, and the positional parameters are shown in Tables 2–4.

Spectral and Magnetic Measurements. The IR spectra were recorded on a Nicolet Avatar FTIR spectrophotometer in a KBr pellet. The magnetic measurements were carried out with a VSM magnetometer in the temperature range 2–250 K up to 9 T.

Results and Discussion

Structures. The novel dimeric silicotungstates $[\{SiMn_2W_9O_{34}(H_2O)\}_2]^{12-}$ (**SiMn$_2$W$_9$**), $[\{SiCu_2W_9O_{34}(H_2O)\}_2]^{12-}$ (**SiCu$_2$W$_9$**), and $[\{SiZn_2W_9O_{34}(H_2O)\}_2]^{12-}$ (**SiZn$_2$W$_9$**) consist of two lacunary $B\text{-}\alpha\text{-}[SiW_9O_{34}]^{10-}$ Keggin moieties linked via a rhomblike M_4O_{16} (M = Mn, Cu, Zn) group leading to a sandwich-type structure (see Figures 1 and 2). This structural type had first been described by Weakley et al. for

Table 2. Fractional Atomic Coordinates ($\times 10^4$) and Equivalent Isotropic Displacement Parameters ($\text{Å}^2 \times 10^3$) for K$_4$Na$_6$Mn[{SiMn$_2$W$_9$O$_{34}$(H$_2$O)}$_2$]·33H$_2$O (**1**)

atom	x/a	y/b	z/c	U(eq)^a	atom	x/a	y/b	z/c	U(eq)^a
W(1)	551(1)	7387(1)	4333(1)	15(1)	Mn(1)	−1970(1)	9681(1)	1102(1)	14(1)
W(2)	2567(1)	9065(1)	3317(1)	15(1)	Mn(2)	−243(1)	11137(1)	209(1)	13(1)
W(3)	3150(1)	6431(1)	2841(1)	15(1)	Mn(3)^b	−4392(3)	10991(3)	4852(3)	26(1)
W(4)	−1721(1)	9579(1)	3404(1)	14(1)	K(1)	241(4)	14103(3)	3003(2)	55(1)
W(5)	283(1)	11243(1)	2373(1)	14(1)	K(2)	0	10000	5000	25(1)
W(6)	2640(1)	10373(1)	1037(1)	13(1)	K(3)^b	−2027(9)	13640(7)	978(6)	79(3)
W(7)	3207(1)	7767(1)	562(1)	13(1)	Na(1)	3659(4)	12835(4)	−452(4)	38(1)
W(8)	1341(1)	6286(1)	1485(1)	14(1)	Na(2)	5416(4)	7183(3)	−1570(3)	22(1)
W(9)	−1221(1)	7210(1)	2970(1)	15(1)	Na(3)	5000	5000	5000	44(2)
					Na(4)^b	−3520(12)	5774(13)	2938(9)	63(4)

atom	x/a	y/b	z/c	U(iso)	atom	x/a	y/b	z/c	U(iso)
Si	689(2)	8792(2)	1901(2)	11(1)	O(78)	2733(6)	6517(6)	669(5)	17(2)
O(1Si)	−145(6)	8403(5)	2814(5)	14(1)	O(7Mn)	2091(6)	8681(5)	−204(5)	14(1)
O(2Si)	1312(6)	9584(5)	2090(5)	14(1)	O(7T)	4448(6)	7564(6)	−168(5)	20(2)
O(3Si)	1718(6)	7700(5)	1740(5)	14(1)	O(89)	212(6)	6348(6)	2480(5)	18(2)
O(4Si)	−89(5)	9430(5)	1013(5)	13(1)	O(8M2)	412(6)	7262(6)	634(5)	17(2)
O(12)	1430(6)	8407(6)	4043(5)	19(2)	O(8T)	1396(6)	5050(6)	1367(5)	21(2)
O(13)	1851(6)	6577(6)	3710(5)	17(2)	O(9M1)	−1696(6)	8034(6)	1862(5)	18(2)
O(14)	−783(6)	8547(5)	4480(5)	16(1)	O(9T)	−2022(7)	6295(6)	3305(6)	26(2)
O(19)	−368(6)	6639(6)	4140(5)	20(2)	O(1W)	−4304(9)	12583(8)	3772(8)	49(3)
O(1MW)	−3846(6)	9852(6)	1188(5)	20(2)	O(2W)	4273(8)	12188(8)	−1837(7)	42(2)
O(1T)	858(7)	6694(6)	5449(6)	26(2)	O(3W)	1772(9)	13257(9)	−809(8)	54(3)
O(23)	3231(6)	7737(6)	3018(5)	21(2)	O(4W)	1541(8)	14301(8)	4246(7)	41(2)
O(25)	1484(6)	10436(5)	3321(5)	16(1)	O(5W)	3777(11)	14576(10)	−1485(9)	64(3)
O(26)	3344(6)	9743(6)	2253(5)	19(2)	O(6W)	6661(13)	4030(12)	4197(11)	84(4)
O(2T)	3461(6)	8875(6)	4134(6)	24(2)	O(7W)	7211(7)	6868(6)	−1000(6)	25(2)
O(37)	3985(6)	6799(6)	1722(5)	19(2)	O(8W)	5273(7)	9050(7)	−2364(6)	29(2)
O(38)	2545(6)	5576(6)	2440(5)	18(2)	O(9W)	2089(7)	11959(7)	3847(6)	30(2)
O(3T)	4239(7)	5447(6)	3500(6)	26(2)	O(10W)	6430(7)	6651(7)	−2916(6)	33(2)
O(45)	−673(6)	10424(6)	3219(5)	17(2)	O(11W)	−5602(8)	10643(7)	4147(7)	36(2)
O(49)	−2178(6)	8292(6)	3547(5)	17(2)	O(12W)	3504(8)	7646(8)	−2078(7)	41(2)
O(4M1)	−2209(6)	10206(5)	2269(5)	17(1)	O(13W)	5364(8)	5363(8)	−934(7)	42(2)
O(4T)	−2846(6)	10201(6)	4068(5)	20(2)	O(14W)^b	−5970(20)	11980(20)	5391(19)	66(7)
O(56)	1652(6)	11483(6)	1562(5)	19(2)	O(15W)^b	−6447(13)	12563(13)	5025(11)	22(3)
O(5M2)	−535(6)	11550(6)	1435(6)	17(2)	O(16W)^b	5386(14)	6624(13)	4107(12)	30(4)
O(5T)	−197(6)	12442(6)	2663(5)	21(2)	O(17W)^b	6550(20)	5920(20)	4770(20)	75(7)
O(67)	3334(6)	8935(5)	921(5)	16(1)	O(18W)^b	−100(40)	4670(30)	220(30)	124(14)
O(6Mn)	1640(6)	10729(5)	174(5)	14(1)	O(19W)^b	−1710(30)	14720(30)	2320(30)	104(10)
O(6T)	3705(6)	10981(6)	452(5)	17(2)	O(20W)^b	−980(40)	4750(30)	1510(30)	134(14)

^{a} U(eq) is defined as one-third of the trace of the orthogonalized $\mathbf{U}_{ij}$ tensor. ^{b} Occupancy 0.5.

[Co$_4$(H$_2$O)$_2$(PW$_9$O$_{34}$)$_2$]$^{10-}$, which is a phosphotungstate derived from the lacunary Keggin ion.[13] Later Finke et al. reported on an analogous structural type based on the lacunary Wells−Dawson ion, [M$_4$(H$_2$O)$_2$(P$_2$W$_{15}$O$_{56}$)$_2$]$^{16-}$ (M = Co^{2+}, Cu^{2+}, Zn^{2+}).[14] By now the interaction of a variety of first-row transition metals with both the lacunary Keggin and Wells−Dawson anions has been studied leading to a family of sandwich-type phosphotungstates.[15]

The synthesis of these structures is based on reaction of transition metal ions with the trivacant B-type phosphotungstates B-α-[PW$_9$O$_{34}$]$^{9-}$ and B-α-[P$_2$W$_{15}$O$_{56}$]$^{12-}$, respectively. Since the analogous lacunary silicotungstates B-α-[SiW$_9$O$_{34}$]$^{10-}$ and B-α-[Si$_2$W$_{15}$O$_{56}$]$^{13-}$, respectively, have not been isolated yet, a rational synthesis of sandwich-type silicotungstates could not be envisioned. It was therefore surprising that **1**, **2**, and **3** could be synthesized starting with [γ-SiW$_{10}$O$_{36}$]$^{8-}$, which means that the mechanism of the metal insertion reaction must be accompanied by isomerization ([γ-SiW$_{10}$O$_{36}$]$^{8-}$ → B-α-[SiW$_9$O$_{34}$]$^{10-}$) and dimerization as well as loss of tungsten. It may be possible to learn more about the mechanism of formation of **SiMn$_2$W$_9$**, **SiCu$_2$W$_9$**, and **SiZn$_2$W$_9$** by comparing their structure with that of the dimeric Ni-substituted β-Keggin

silicotungstate, [{β-SiNi$_2$W$_{10}$O$_{36}$(OH)$_2$(H$_2$O)}$_2$]$^{12-}$ (**SiNi$_2$W$_{10}$**), recently reported by Kortz et al.[10] The anion **SiNi$_2$W$_{10}$** was synthesized by reacting Ni^{2+} ions with [γ-SiW$_{10}$O$_{36}$]$^{8-}$ under conditions very similar to those used for the synthesis of **SiMn$_2$W$_9$**, **SiCu$_2$W$_9$**, and **SiZn$_2$W$_9$**. However, we were not able to synthesize [{SiNi$_2$W$_9$O$_{34}$(H$_2$O)}$_2$]$^{12-}$ (**SiNi$_2$W$_9$**) under the conditions studied. Nevertheless, it can be helpful to imagine rearrangement of **SiNi$_2$W$_{10}$** accompanied by loss of two W atoms leading to [{SiNi$_2$W$_9$O$_{34}$(H$_2$O)}$_2$]$^{12-}$ (**SiNi$_2$W$_9$**) according to the following equation: [{β-SiNi$_2$W$_{10}$O$_{36}$(OH)$_2$(H$_2$O)}$_2$]$^{12-}$

(13) Weakley, T. J. R.; Evans, H. T., Jr.; Showell, J. S.; Tourné, G. F.; Tourné, C. M. *J. Chem. Soc., Chem. Commun.* **1973**, 139.

(14) Finke, R. G.; Droege, M. W. *Inorg. Chem.* **1983**, 22, 1006.

(15) (a) Finke, R. G.; Droege, M.; Hutchinson, J. R.; Gansow, O. *J. Am. Chem. Soc.* **1981**, *103*, 1587. (b) Evans, H. T.; Tourné, C. M.; Tourné, G. F.; Weakley, T. J. R. *J. Chem. Soc., Dalton Trans.* **1986**, 2699. (c) Finke, R. G.; Droege, M. W.; Domaille, P. J. *Inorg. Chem.* **1987**, 26, 3886. (d) Wasfi, S. H.; Rheingold, A. L.; Kokoszka, G. F.; Goldstein, A. S. *Inorg. Chem.* **1987**, 26, 2934. (e) Weakley, T. J. R.; Finke, R. G. *Inorg. Chem.* **1990**, *29*, 1235. (f) Gómez-García, C. J.; Coronado, E.; Borrás-Almenar, J. J. *Inorg. Chem.* **1992**, *31*, 1667. (g) Casañ-Pastor, N.; Bas-Serra, J.; Coronado, E.; Pourroy, G.; Baker, L. C. W. *J. Am. Chem. Soc.* **1992**, *114*, 10380. (h) Gómez-García, C. J.; Coronado, E.; Gómez-Romero, P.; Casañ-Pastor, N. *Inorg. Chem.* **1993**, *32*, 3378. (i) Gómez-García, C. J.; Borrás-Almenar, J. J.; Coronado, E.; Ouahab, L. *Inorg. Chem.* **1994**, *33*, 4016. (j) Zhang, X.-Y.; Jameson, G. B.; O'Connor, C. J.; Pope, M. T. *Polyhedron* **1996**, *15*, 917. (k) Zhang, X.; Chen, Q.; Duncan, D. C.; Campana, C.; Hill, C. L. *Inorg. Chem.* **1997**, *36*, 4208. (l) Zhang, X.; Chen, Q.; Duncan, D. C.; Lachicotte, R. J.; Hill, C. L. *Inorg. Chem.* **1997**, *36*, 4381. (m) Clemente-Juan, J. M.; Coronado, E.; Galán-Mascarós, J. R.; Gómez-García, C. J. *Inorg. Chem.* **1999**, *38*, 55.

Table 3. Fractional Atomic Coordinates ($\times 10^4$) and Equivalent Isotropic Displacement Parameters ($\text{Å}^2 \times 10^3$) for K$_3$Na$_5$[{SiCu$_2$W$_9$O$_{34}$(H$_2$O)}$_2$]·26H$_2$O (**2**)

atom	x/a	y/b	z/c	U(eq)^a	atom	x/a	y/b	z/c	U(eq)^a
W(1)	2133(1)	5130(1)	4106(1)	17(1)	Cu(1)	4724(2)	2978(2)	1009(1)	16(1)
W(2)	1022(1)	7594(1)	2582(1)	16(1)	Cu(2)	3822(2)	5086(2)	−280(1)	14(1)
W(3)	3988(1)	7331(1)	3296(1)	16(1)	K(1)	5000	5000	5000	31(1)
W(4)	1992(1)	3438(1)	2628(1)	16(1)	K(2)	−850(4)	3583(4)	1338(4)	40(1)
W(5)	926(1)	5872(1)	1100(1)	15(1)	Na(1)	687(6)	4432(6)	6654(5)	28(2)
W(6)	2463(1)	7926(1)	372(1)	15(1)	Na(2)	8155(6)	8977(6)	−113(6)	32(2)
W(7)	5364(1)	7711(1)	1078(1)	15(1)	Na(3)^b	−251(19)	1455(18)	4063(19)	86(9)
W(8)	6421(1)	5445(1)	2398(1)	15(1)					
W(9)	4628(1)	3246(1)	3276(1)	17(1)					

atom	x/a	y/b	z/c	U(iso)	atom	x/a	y/b	z/c	U(iso)
Si	3676(3)	5567(3)	1762(3)	10(1)	O(7Cu)	5724(9)	6893(8)	185(8)	15(2)
O(1Si)	3261(9)	4661(8)	2611(8)	14(2)	O(7T)	6026(10)	8833(9)	590(9)	23(3)
O(2Si)	2442(9)	6434(9)	1547(8)	18(2)	O(89)	5561(9)	4379(9)	3178(8)	17(2)
O(3Si)	4549(9)	6256(9)	2057(8)	20(2)	O(8C2)	6685(9)	4753(8)	1437(8)	16(2)
O(4Si)	4418(9)	4954(9)	862(8)	18(2)	O(8T)	7828(10)	5072(9)	2735(9)	25(3)
O(12)	1151(9)	6297(8)	3477(8)	15(2)	O(9C1)	5262(9)	2916(9)	2135(8)	18(2)
O(13)	3241(9)	6124(8)	3930(8)	16(2)	O(9T)	5429(10)	2199(9)	3924(9)	25(3)
O(14)	1326(10)	4146(9)	3788(8)	21(3)	O(1W)	2469(13)	2972(12)	6128(11)	43(4)
O(19)	3450(9)	3982(9)	4312(8)	17(2)	O(2W)	8487(10)	7180(9)	−447(9)	24(3)
O(1CW)	4898(11)	1023(10)	1252(9)	30(3)	O(3W)	7386(11)	9623(10)	−1518(10)	31(3)
O(1T)	1404(10)	5253(9)	5189(9)	22(3)	O(4W)	8200(11)	8360(10)	1451(10)	31(3)
O(23)	2435(9)	7834(9)	2909(8)	20(2)	O(5W)	10019(12)	9442(11)	−1038(11)	40(3)
O(25)	107(9)	6868(9)	2053(8)	17(2)	O(6W)^b	250(30)	730(30)	2760(30)	58(9)
O(26)	1323(9)	8498(8)	1514(8)	16(2)	O(7W)^b	−2230(20)	2070(20)	2205(18)	28(6)
O(2T)	−129(10)	8465(9)	3204(9)	22(3)	O(8W)^b	4110(20)	9340(20)	4980(20)	40(7)
O(37)	4670(9)	8230(8)	2303(8)	16(2)	O(9W)^b	7920(20)	2850(20)	4010(20)	33(6)
O(38)	5561(9)	6429(9)	3367(8)	19(2)	O(10W)^b	740(30)	2340(30)	4990(20)	54(9)
O(3T)	3780(10)	8094(9)	4172(9)	26(3)	O(11W)^b	−2160(30)	8800(20)	4000(20)	49(8)
O(45)	1002(9)	4719(9)	2093(8)	18(2)	O(12W)^b	1440(40)	30(40)	3590(40)	104(16)
O(49)	3193(10)	2623(9)	3308(8)	20(3)	O(13W)^b	−2840(40)	10100(40)	2570(30)	88(14)
O(4C1)	2991(9)	3109(9)	1580(8)	18(2)	O(14W)^b	−5340(30)	10170(30)	3050(30)	61(9)
O(4T)	984(10)	2542(9)	2842(9)	25(3)	O(15W)^b	3750(30)	10370(30)	3470(30)	55(9)
O(56)	1137(10)	7257(9)	331(8)	21(3)	O(16W)^b	2810(30)	10730(30)	4350(30)	68(10)
O(5C2)	2128(10)	5129(9)	342(8)	22(3)	O(17W)^b	−1520(40)	610(30)	3450(30)	82(12)
O(5T)	−393(9)	5706(9)	796(8)	17(2)	O(18W)^b	5940(50)	9200(50)	4280(40)	130(20)
O(67)	3705(9)	8212(9)	907(8)	17(2)	O(19W)^b	−180(30)	2610(30)	4770(30)	61(10)
O(6Cu)	3584(9)	7037(8)	−342(8)	17(2)	O(20W)^b	−3480(50)	10000(50)	2290(40)	130(20)
O(6T)	2166(9)	9154(9)	−339(8)	19(2)	O(21W)^b	1120(50)	−400(50)	4270(40)	125(19)
O(78)	6662(9)	6833(9)	1666(8)	19(2)					

^{a} U(eq) is defined as one-third of the trace of the orthogonalized $\mathbf{U}_{ij}$ tensor. ^{b} Occupancy 0.5.

→ [{SiNi$_2$W$_9$O$_{34}$(H$_2$O)}$_2$]$^{12-}$ + 2H$_2$WO$_4$. Based on experimental work **SiNi$_2$W$_9$** is less stable than **SiNi$_2$W$_{10}$**, but the situation is the reverse for manganese, copper, and zinc. Apparently **SiMn$_2$W$_9$**, **SiCu$_2$W$_9$**, and **SiZn$_2$W$_9$** are more stable than their respective intermediates [{β-SiMn$_2$W$_{10}$O$_{36}$(OH)$_2$(H$_2$O)}$_2$]$^{12-}$ (**SiMn$_2$W$_{10}$**), [{β-SiCu$_2$W$_{10}$O$_{36}$(OH)$_2$(H$_2$O)}$_2$]$^{12-}$ (**SiCu$_2$W$_{10}$**), and [{β-SiZn$_2$W$_{10}$O$_{36}$(OH)$_2$(H$_2$O)}$_2$]$^{12-}$ (**SiZn$_2$W$_{10}$**), for which we have spectroscopic evidence. However, we could not crystallize **SiMn$_2$W$_{10}$**, **SiCu$_2$W$_{10}$**, and **SiZn$_2$W$_{10}$** due to rearrangement to **SiMn$_2$W$_9$**, **SiCu$_2$W$_9$**, and **SiZn$_2$W$_9$**, respectively. Tungstic acid being released according to the above equation most likely leads to the formation of isopolytungstates.

The dimeric **SiMn$_2$W$_9$**, **SiCu$_2$W$_9$**, and **SiZn$_2$W$_9$** are structurally equivalent to their phosphorus-containing analogues [{PMn$_2$W$_9$O$_{34}$(H$_2$O)}$_2$]$^{10-}$, [{PCu$_2$W$_9$O$_{34}$(H$_2$O)}$_2$]$^{10-}$, and [{PZn$_2$W$_9$O$_{34}$(H$_2$O)}$_2$]$^{10-}$. The main difference is the charge, and since **SiMn$_2$W$_9$**, **SiCu$_2$W$_9$**, and **SiZn$_2$W$_9$** are 12− ions, it was expected to find the appropriate number of cations for charge-balance considerations. Bond-valence sum calculations for **SiMn$_2$W$_9$**, **SiCu$_2$W$_9$**, and **SiZn$_2$W$_9$** indicated that the terminal oxygen atoms associated with two of the four transition metal ions in the belt are the only protonation sites of the polyanions.[16] However, only in the case of **1** is charge balance

fully satisfied as a result of single-crystal X-ray crystallography. It is of interest to note that in addition to four potassium and six sodium ions there is one Mn^{2+} ion present as a countercation besides the four Mn^{2+} ions bound within each **SiMn$_2$W$_9$**. This observation was confirmed by elemental analysis and by magnetic studies of **1**. In the case of **2** and **3** not all cations could be identified crystallographically, most likely because of disorder, which is not uncommon for these kinds of compounds. However, the quality of the elemental analyses for **2** and **3** is good enough to indicate that potassium and sodium are the only cations present in both compounds. For **2** this is confirmed by the magnetic data, which do not give any indication for Cu^{2+} countercations to be present.

Magnetic Properties. Since **SiMn$_2$W$_9$** and **SiCu$_2$W$_9$** contain a well-isolated central M$_4$O$_{16}$ (M = Mn^{2+}, Cu^{2+}) unit, it is of interest to investigate the magnetic properties of **1** and **2**. Magnetization and magnetic susceptibility measurements are efficient methods to obtain information about the magnetic interactions in spin clusters. The results of the magnetic measurements for **1** and **2** are displayed in Figures 3−6. The magnetization of **1** at 2 K shows a steep increase up to about 2 T and then continues linearly without reaching saturation up to 9 T (see Figure 3). The temperature dependence of the magnetic susceptibility of **1** shows an almost constant value of 1.9×10^{-3} emu/g with a slight increase going from 250 to 100 K

(16) Brown, I. D.; Altermatt, D. *Acta Crystallogr.* **1985**, *B41*, 244.

Table 4. Fractional Atomic Coordinates ($\times 10^4$) and Equivalent Isotropic Displacement Parameters (Å^2 x 10^3) for $K_4Na_6[\{SiZn_2W_9O_{34}(H_2O)\}_2]\cdot 34H_2O$ (**3**)

atom	x/a	y/b	z/c	U(eq)[a]	atom	x/a	y/b	z/c	U(eq)[a]
W(1)	986(1)	3178(1)	1427(1)	12(1)	Zn(1)	2679(1)	4646(1)	5004(1)	11(1)
W(2)	3453(1)	2147(1)	1527(1)	10(1)	Zn(2)	4765(1)	3806(1)	5108(1)	10(1)
W(3)	3966(1)	5021(1)	1250(1)	9(1)	K(1)	6404(3)	3803(2)	1116(2)	18(1)
W(4)	626(1)	2491(1)	3340(1)	15(1)	K(2)[b]	4542(11)	9949(8)	2117(7)	61(3)
W(5)	3063(1)	1480(1)	3445(1)	13(1)	K(3)[b]	−927(8)	3411(8)	4817(6)	47(2)
W(6)	5787(1)	3091(1)	3278(1)	10(1)	Na(1)	3499(5)	1103(4)	−835(4)	20(1)
W(7)	6321(1)	5922(1)	2994(1)	9(1)	Na(2)	−262(5)	−2577(5)	2825(4)	23(1)
W(8)	4108(1)	6867(1)	2942(1)	10(1)	Na(3)	−949(5)	2247(4)	−1036(4)	21(1)
W(9)	1072(1)	5058(1)	3069(1)	13(1)					

atom	x/a	y/b	z/c	U(iso)	atom	x/a	y/b	z/c	U(iso)
Si(1)	3530(3)	4186(2)	3249(2)	8(1)	O(7Zn)	6366(7)	5986(7)	4118(6)	11(2)
O(1Si)	2076(7)	3849(7)	2887(6)	11(2)	O(7T)	7803(8)	6586(7)	2997(6)	18(2)
O(2Si)	3839(7)	3109(7)	2974(6)	12(2)	O(89)	2413(7)	6091(7)	2738(6)	12(2)
O(3Si)	4232(7)	5159(6)	2766(5)	7(1)	O(8Z2)	4381(7)	6883(7)	4055(6)	14(2)
O(4Si)	3947(7)	4603(6)	4285(5)	9(2)	O(8T)	4181(8)	8187(8)	2911(7)	20(2)
O(12)	1935(8)	2306(7)	1391(6)	15(2)	O(9Z1)	1952(8)	5461(7)	4190(6)	15(2)
O(13)	2321(8)	4315(7)	1230(6)	15(2)	O(9T)	156(8)	5790(8)	3058(7)	21(2)
O(14)	78(8)	2264(7)	2059(6)	18(2)	O(1W)	4238(10)	−338(9)	−855(8)	31(2)
O(19)	502(8)	4329(7)	1848(6)	18(2)	O(2W)	−2668(10)	1211(9)	−534(8)	31(2)
O(1ZW)	1404(8)	4693(7)	5710(6)	19(2)	O(3W)	−599(10)	−887(10)	2656(8)	34(3)
O(1T)	15(8)	2713(7)	437(6)	17(2)	O(4W)	−1451(9)	3824(8)	−915(7)	22(2)
O(23)	3993(7)	3560(7)	1220(6)	10(2)	O(5W)	1378(9)	5369(8)	−789(7)	24(2)
O(25)	2897(8)	1087(7)	2172(6)	15(2)	O(6W)	7618(10)	2454(10)	1719(8)	35(3)
O(26)	5045(7)	2387(7)	2051(6)	13(2)	O(7W)	963(9)	3172(8)	−1319(7)	25(2)
O(2T)	3251(8)	1327(7)	574(6)	19(2)	O(8W)	5646(9)	2266(9)	−447(7)	27(2)
O(37)	5648(7)	5592(7)	1719(6)	12(2)	O(9W)	1677(9)	−365(9)	−891(7)	28(2)
O(38)	3875(7)	6382(7)	1668(6)	11(2)	O(10W)	−1669(8)	1918(8)	−2559(7)	20(2)
O(3T)	3920(8)	5132(7)	208(6)	15(2)	O(11W)	3005(10)	1058(9)	−2319(8)	32(2)
O(45)	1551(8)	1619(7)	3139(6)	17(2)	O(12W)	3166(8)	2818(8)	−780(7)	20(2)
O(49)	63(8)	3700(7)	3280(6)	18(2)	O(13W)	684(9)	−594(8)	1421(7)	27(2)
O(4Z1)	1507(7)	3104(7)	4407(6)	13(2)	O(14W)[b]	590(20)	−1724(19)	4335(16)	35(5)
O(4T)	−636(9)	1494(8)	3486(7)	26(2)	O(15W)[b]	3015(17)	−600(16)	6490(13)	21(4)
O(56)	4761(8)	1722(7)	3463(6)	15(2)	O(16W)[b]	327(19)	416(17)	97(15)	29(5)
O(5Z2)	3507(8)	2305(7)	4469(6)	15(2)	O(17W)[b]	5843(15)	9287(14)	4589(12)	15(3)
O(5T)	2609(8)	160(7)	3643(6)	17(2)	O(18W)[b]	2710(19)	−398(17)	5002(14)	27(4)
O(67)	6215(7)	4449(6)	2844(6)	10(2)	O(19W)[b]	3680(20)	8540(20)	4887(18)	42(6)
O(6Zn)	5975(7)	3821(7)	4327(6)	13(2)	O(20W)[b]	1770(20)	1210(20)	5495(17)	37(5)
O(6T)	7084(8)	2837(7)	3346(6)	16(2)	O(21W)[b]	−20(40)	−140(30)	4130(30)	87(12)
O(78)	5788(7)	7135(7)	2959(6)	13(2)					

[a] U(eq) is defined as one-third of the trace of the orthogonalized $\mathbf{U}_{ij}$ tensor. [b] Occupancy 0.5.
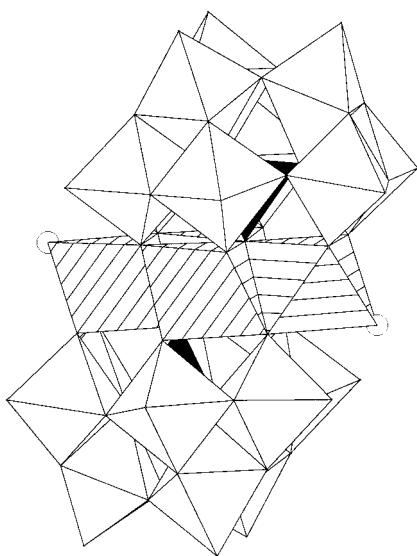

Figure 1. Polyhedral representation of $[\{SiM_2W_9O_{34}(H_2O)\}_2]^{12-}$ (M = Mn^{2+}, Cu^{2+}, Zn^{2+}). The small, empty spheres represent water molecules.

Figure 2. Ball and stick representation of a half-unit of $[\{SiMn_2W_9O_{34}(H_2O)\}_2]^{12-}$ (**Si$_2$Mn$_2$W$_9$**) showing 50% probability ellipsoids and the labeling scheme.

(see Figure 4). This tendency becomes more pronounced below 100 K, leading to an exponential increase between 50 and 15
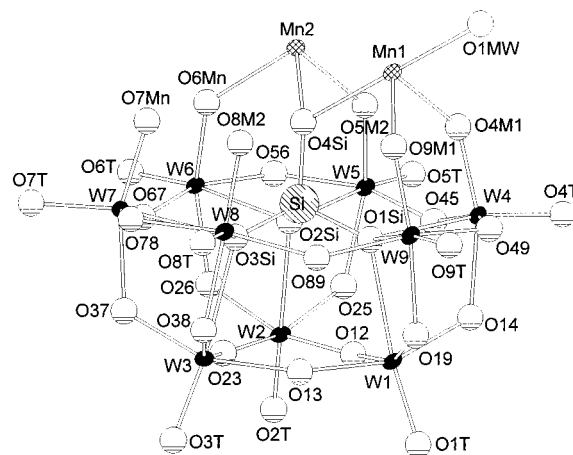
K, and below 15 K there is a sharp increase to reach a value of 3.7×10^{-2} emu/g at 2 K.

The magnetic behavior of **2** is clearly different from that of **1**. The magnetization of **2** reaches saturation at 5 T due to weak antiferromagnetic coupling (see Figure 5). The magnetic
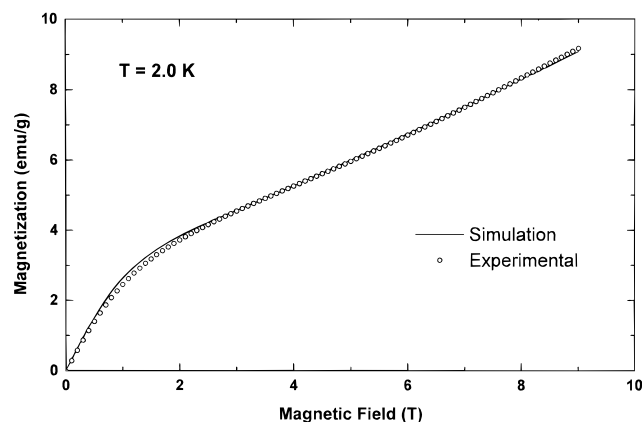
Figure 3. Plot of magnetization of $K_4Na_6Mn[\{SiMn_2W_9O_{34}(H_2O)\}_2]\cdot$ $33H_2O$ (**1**) at 2 K.
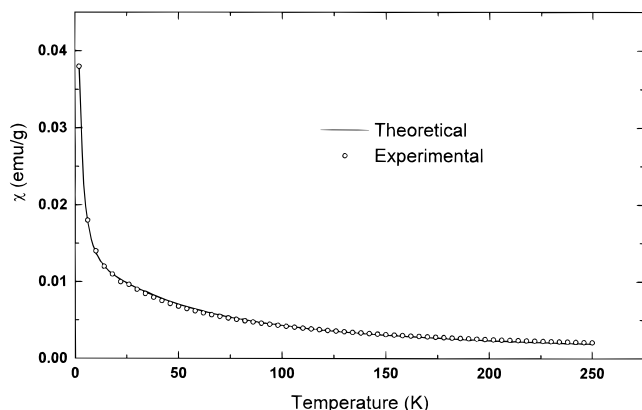
Figure 4. Plot of the effective magnetic moment as a function of temperature for $K_4Na_6Mn[\{SiMn_2W_9O_{34}(H_2O)\}_2]\cdot33H_2O$ (**1**) in a constant magnetic field of 1 T.
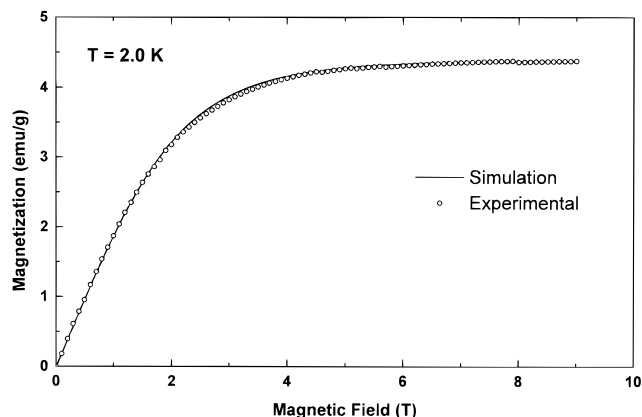
Figure 5. Plot of magnetization of $K_3Na_5[\{SiCu_2W_9O_{34}(H_2O)\}_2]\cdot$ $26H_2O$ (**2**) at 2 K.

Figure 6. Plot of the effective magnetic moment as a function of temperature for $K_3Na_5[\{SiCu_2W_9O_{34}(H_2O)\}_2]\cdot26H_2O$ (**2**) in a constant magnetic field of 1 T.

**Table 5.** Selected Distances (Å), Angles (deg), and Exchange Parameters within the Tetrameric M_4O_{16} (M = Mn, Cu, Zn) Units of $K_4Na_6Mn[\{SiMn_2W_9O_{34}(H_2O)\}_2]\cdot33H_2O$ (**1**), $K_3Na_5[\{SiCu_2W_9O_{34}(H_2O)\}_2]\cdot26H_2O$ (**2**), $K_4Na_6[\{SiZn_2W_9O_{34}(H_2O)\}_2]\cdot34H_2O$ (**3**), $K_{10}[Mn_4(H_2O)_2(PW_9O_{34})_2]\cdot20H_2O$ (**1a**), and $K_8Na_2[Cu_4(H_2O)_2(PW_9O_{34})_2]\cdot16H_2O$ (**2a**)

	1[a]	**1a**[b]	**2**[a]	**2a**[c,d]	**3**[a]
M1−O4X[e] (Å)	2.196(6)	2.27	2.414(11)	2.55(1)	2.128(8)
M1−O6M (Å)	2.184(7)	2.18	1.960(10)	1.96(1)	2.126(9)
M1−O7M (Å)	2.176(7)	2.14	1.984(12)	1.94(1)	2.106(8)
M2−O4X (Å)	2.207(7)	2.34	1.992(12)	2.05(1)	2.113(8)
M2−O4X* (Å)	2.218(7)	2.32	1.991(10)	2.05(1)	2.130(8)
M2−O6M (Å)	2.176(7)	2.13	2.399(10)	2.35(1)	2.126(9)
M2−O7M (Å)	2.191(7)	2.14	2.416(10)	2.36(1)	2.108(8)
M1···M2=M1*···M2* (Å)	3.212(2)	3.294	3.162(3)	3.246(4)	3.111(2)
M1···M2*=M1*···M2 (Å)	3.216(2)	3.290	3.163(3)	3.263(4)	3.144(2)
M2···M2* (Å)	3.232(3)	3.447	2.965(4)	3.087(4)	3.089(3)
M1···M1* (Å)	5.556(4)	5.609	5.588(5)	5.724	5.439(4)
M1−O4X−M2 (deg)	93.7(2)	91.4	91.2(4)	89.2	94.4(3)
M1−O4X−M2* (deg)	93.5(3)	91.6	91.2(4)	89.6	95.2(3)
M2−O4X−M2* (deg)	93.8(3)	95.5	96.2(5)	97.6	93.4(3)
M1−O6M−M2 (deg)	95.0(3)	99.6	92.5(4)	98.2	95.4(4)
M1−O7M−M2 (deg)	94.7(3)	100.6	91.4(4)	97.6	95.2(4)
J (cm^{-1})	−1.77(5)	−1.7	−0.10(2)	−3.5	
J' (cm^{-1})	0.08(2)	0.3	−0.29(2)	−12.5	

[a] This work. [b] Reference 15h. [c] Reference 15e. [d] Reference 15f. [e] X = Si (**1**, **2**, **3**); X = P (**1a**, **2a**).

M−O−M angles, and four types of M···M distances. The bond lengths and angles of this M_4O_6 (M = Mn^{2+}, Cu^{2+}) core determine the magnetic properties of the polyoxoanion (see Table 5).

In order to analyze the observed magnetic properties of **1** and **2** the following exchange scheme has been used:
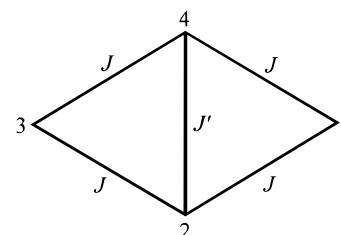
The corners of the rhomb with the numbers 1, 2, 3, and 4 symbolize the transition metal ions Mn1, Mn2, Mn1′, and Mn2′ as well as Cu1, Cu2, Cu1′, and Cu2′, respectively. The

susceptibility of **2** shows an almost constant value of 2.5×10^{-4} emu/g between 300 and 50 K (see Figure 6). There is an exponential increase between 50 and 20 K leading to a sharp increase below 20 K to reach a value of 1.3×10^{-2} emu/g at 5 K.

The exchange interaction between the individual metal ions of each tetrameric Mn_4O_{16} unit in **SiMn₂W₉** and Cu_4O_{16} unit in **SiCu₂W₉** is mediated through M−O−M (M = Mn^{2+}, Cu^{2+}) linkages. In each M_4O_{16} unit (M = Mn^{2+}, Cu^{2+}) there are two μ_3-oxo bridges (O4Si and O4Si′) and four μ_2-oxo bridges (O6M, O6M′, O7M, O7M′) linking the four transition metal ions. This results in seven types of M−O bond distances, five types of

interaction between M1 and M2 and between M1′ and M2 is described by the coupling constant J, and the interaction between M2 and M2′ is given by the coupling constant J'.

In the presence of an external magnetic field the spin Hamiltonian for the tetrameric cluster is given by

$$H = g\mu_B(S_1 + S_2 + S_3 + S_4)H - 2J'S_2S_4 - 2J(S_1S_2 + S_1S_4 + S_2S_3 + S_3S_4) \quad (1)$$

where g is the Landé factor (2.0 for Mn^{2+} and 2.3 for Cu^{2+}),[17] μ_B is the Bohr magneton and H is the external magnetic field. The energy levels of the spin Hamiltonian of eq 1 are given by

$$E(S_T, S_{12}, S_{34}, S_{24}, m, m') = -(m + m')g\mu_B H + J'[S_{24}(S_{24} + 1) - 2S(S + 1)] + J[(S_T(S_T + 1) - S_{12}(S_{12} + 1) - S_{34}(S_{34} + 1)] \quad (2)$$

where $S_T = S_1 + S_2 + S_3 + S_4$ and $S_{kl} = S_k + S_l$ with $k,l = 1$, 2, 3, 4. For the M_4O_6 core in **SiMn₂W₉** we have $S_1 = S_2 = S_3 = S_4 = 5/2$, $0 \le S_{12} \le 5$, $0 \le S_{34} \le 5$ and $|S_{12} - S_{34}| \le S_T \le S_{12} + S_{34}$, and for **SiCu₂W₉** we have $S_1 = S_2 = S_3 = S_4 = 1/2$, $0 \le S_{12} \le 1$, $0 \le S_{34} \le 1$ and $|S_{12} - S_{34}| \le S_T \le S_{12} + S_{34}$. The value of the magnetization was then calculated by using its thermodynamic definition:

$$M = -k_B N_A T(\partial \ln(Z)/\partial H) \quad (3)$$

where Z is the partition function given by

$$Z = \sum_{i,j} e^{-E_{i,j}/k_B T} \quad (4)$$

The magnetization measurements of **1** and **2** at 2 K are shown in Figures 3 and 5, respectively. The experimental data were fitted using eq 3, and the values of the exchange interactions were determined to be $J = -1.77(5)$ cm⁻¹ and $J' = 0.08(2)$ cm⁻¹ for **1** and $J = -0.10(2)$ cm⁻¹ and $J' = -0.29(2)$ cm⁻¹ for **2**.

Fitting of the magnetization data for **1** suggests the existence of isolated Mn^{2+} ions. Based on the magnetic results 16.3(5)% of all the manganese ions in **1** are present as countercations, which is in good agreement with elemental analysis (14.9%). Single-crystal X-ray crystallography also indicated the presence of isolated Mn^{2+} cations (20.0%). The theoretical magnetization of isolated Mn^{2+} ($Mn_{isolated}$) is proportional to the Brillouin function $\beta_s(\xi)$:

$$Mn_{isolated} = N\mu_B g S \beta_s(\xi) \quad (5)$$

$$\beta_s(\xi) = \frac{2S + 1}{2S} \coth\left(\frac{2S + 1}{2S}\xi\right) - \frac{1}{2S} \coth\left(\frac{\xi}{2S}\right) \quad (6)$$

where $\xi = Sg\mu_B H/(k_B T)$ and k_B is the Boltzmann constant.

Figures 7 and 8 show the energy level diagrams versus the ratio J'/J for **1** and **2**, respectively. The energy levels are labeled $E(S_T, S_{13}, S_{24})$ where $S_T = S_{13} + S_{24}$, $S_{13} = S_1 + S_3$ and $S_{24} = S_2 + S_4$. In the case of **1** the total spin of the Mn_4O_{16} unit is a good quantum number ($S_i = 5/2$ with $i = 1, 2, 3, 4$; $S_T = S_1 + S_2 + S_3 + S_4$). The dimension of the spin Hamiltonian matrix is 1296×1296, leading to six singlets, 15 triplets, 21 quintets, 24 septets, 24 9-folds, 21 11-folds, 15 13-folds, 10 15-folds, 6 17-folds, 3 19-folds and one 21-fold. The ratio of J'/J for **1** is -0.04, indicating that the ground state is a singlet state (0, 5, 5). For **2** the spin Hamiltonian matrix dimension is 16×16, leading to two singlets, three triplets, and one quintet. Since
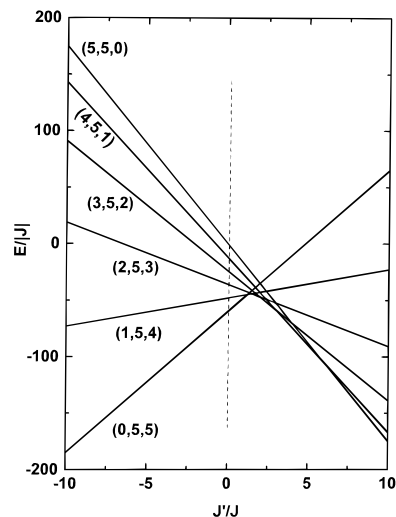
Figure 7. Energy level diagram versus the ratio J'/J for K_4Na_6Mn-[{SiMn₂W₉O₃₄(H₂O)}₂]·33H₂O (**1**). The energy levels are labeled $E(S_T, S_{13}, S_{24})$ where $S_T = S_{13} + S_{24}$, $S_{13} = S_1 + S_3$ and $S_{24} = S_2 + S_4$. The vertical broken line indicates the experimental J'/J value.
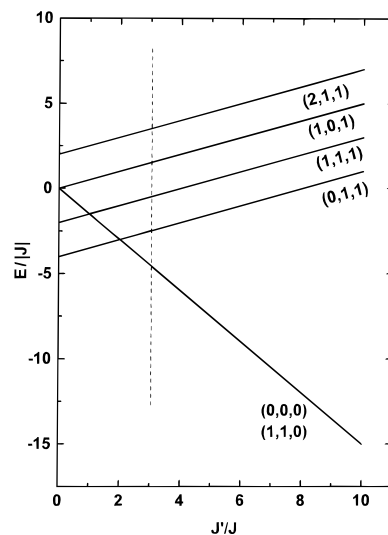
Figure 8. Energy level diagram versus the ratio J'/J for K_3Na_5-[{SiCu₂W₉O₃₄(H₂O)}₂]·26H₂O (**2**). The energy levels are labeled $E(S_T, S_{13}, S_{24})$ where $S_T = S_{13} + S_{24}$, $S_{13} = S_1 + S_3$ and $S_{24} = S_2 + S_4$. The vertical broken line indicates the experimental J'/J value.

$J'/J = 3$, the ground state is a mixture of a singlet state (0, 0, 0) and a triplet state (1, 1, 0).

The magnetic susceptibility per mole is given by Gladfelter et al.:[18]

$$\chi_{cluster} = (4N_A g^2 \mu_B^2/3k_B T)S(S + 1) \frac{\sum_i (2S + 1)S(S + 1)e^{-E_i/k_B T}}{\sum_i (2S + 1)e^{-E_i/k_B T}} \quad (7)$$

The contribution of isolated Mn^{2+} ions to the magnetic susceptibility of **1** is given by

(17) Ginsberg, A. P. *Inorg. Chim. Acta Rev.* **1971**, *5*, 45.
(18) Gladfelter, W. L.; Lynch, M. W.; Schaefer, W. P.; Hendrickson, D. N.; Gray, H. B. *Inorg. Chem.* **1981**, *20*, 2390.

$$\chi_{isolated} = (N_A g^2 \mu_B^2 / 3k_B) S(S+1) \tag{8}$$

Figures 4 and 6 show the magnetic susceptibility for **1** and **2**, respectively, in the temperature range 2–250 K. Dotted lines represent the best fit to the experimental data. The exchange constants obtained were $J = -1.81(5)$ cm^{-1} and $J' = 0.09(2)$ cm^{-1} for **1** and $J = -0.09(2)$ cm^{-1} and $J' = -0.28(2)$ cm^{-1} for **2**. In order to account for intercluster interactions we included the mean field correction, which was found to be weakly antiferromagnetic, $\theta = -0.41$ cm^{-1}.

It is of interest to compare the magnetic properties of **1** and **2** with those of their phosphorus-containing analogues $K_{10}[Mn_4(H_2O)_2(PW_9O_{34})_2] \cdot 20H_2O$ (**1a**) and $K_8Na_2[Cu_4(H_2O)_2(PW_9O_{34})_2] \cdot 16H_2O$ (**2a**), respectively, reported by Coronado et al.[15f,h] As shown in Table 5 the respective coupling constants (in cm^{-1}) are $J = -1.77(5)$ (**1**), -1.7 (**1a**), $-0.10(2)$ (**2**), -3.5 (**2a**) and $J' = 0.08(2)$ (**1**), 0.3 (**1a**), $-0.29(2)$ (**2**), -12.5 (**2a**). The type of magnetic exchange interaction as represented by the sign of the coupling constants J and J' is the same for **1** and **1a** (antiferromagnetic and weakly ferromagnetic) and for **2** and **2a** (antiferromagnetic), respectively. However, with respect to the magnitude of the respective coupling constants some differences are apparent. Coupling along the sides of the rhomb (see exchange scheme) is very similar for **1** and **1a** ($J_{1a}/J_1 = 0.96$), but with respect to coupling along the short diagonal the exchange is more efficient for **1a** ($J'_{1a}/J'_1 = 3.8$). The differences are more pronounced for the copper derivatives **2** and **2a**. For **2a** both coupling constants J and J' are significantly larger than for **2** ($J_{2a}/J_2 = 35.0$, $J'_{2a}/J'_2 = 43.1$), indicating weaker exchange interaction in the copper-substituted silicotungstate compared to the phosphotungstate.

Since the magnetic M_4O_{16} (M = Mn^{2+}, Cu^{2+}) units in neighboring polyoxoanions in the crystalline state are well isolated from each other, intercluster magnetic exchange is very weak compared to intracluster exchange. The observed differences in the magnetic properties of **1** and **1a** and especially **2** and **2a** should therefore be predominantly due to differences in the geometry of the central M_4O_{16} units. The Si–O bond lengths in **1** and **2** are approximately 0.1 Å longer than the related P–O bond lengths in **1a** and **2a**, leading to M–O(Si) (M = Mn, Cu) bonds which are slightly shorter than the corresponding M–O(P) (M = Mn, Cu) bonds. As a result, the four transition metal ions of the rhombic M_4O_{16} (M = Mn, Cu) unit are closer to each other in **1** and **2** than in **1a** and **2a**, respectively (see Table 5). A comparison of the M–O–M (M = Mn, Cu) bond angles of **1** with **1a** and **2** with **2a** shows that two angles are slightly larger (M1–O4X–M2, M1–O4X–M2*), one is slightly smaller (M2–O4X–M2*), and the remaining two are significantly smaller (M1–O6M–M2, M1–O7M–M2) for the silicotungstates than for the phosphotungstates. Therefore the observed trends for **1** and **2** with respect to bond distances and bond angles

are the same for both, which does not explain why the magnetic exchange interaction is so much more efficient for **2a** than for **2**. Coronado et al. pointed out that the efficient magnetic exchange along the diagonal of the rhomb in **2a** is a result of the Jahn–Teller distorted Cu^{2+} ions.[15f] The distortion leads to good overlap of the half-filled $d_{x^2-y^2}$ orbitals of the two central copper ions. Since the respective Cu2–O4–Cu2* angles are 96.2° for **2** and 97.6° for **2a**, it could be expected that J'_2 was larger than J'_{2a}, but the exact opposite is observed ($J'_{2a}/J'_2 = 43.1$).

These results indicate that it can be possible to predict the correct sign of the exchange constants for transition metal substituted polyoxometalates by comparison with structurally related species. However, in order to determine the correct orders of magnitude of the exchange constants experimental work is essential.

Conclusions

Three novel dimeric silicotungstates $[\{SiM_2W_9O_{34}(H_2O)\}_2]^{12-}$ (M = Mn^{2+}, Cu^{2+}, Zn^{2+}) have been synthesized. Single-crystal X-ray diffraction revealed that the polyanions have a sandwich-type structure, which so far had only been known for phosphotungstates. Furthermore they represent only the second structural type of silicotungstates containing four transition metal ions. Magnetic measurements show that the central Mn$_4$ unit in **1** exhibits antiferromagnetic as well as weak ferromagnetic exchange interactions whereas in **2** the exchange interactions are antiferromagnetic.

Formation of the title anions is accomplished by interaction of the divalent transition metal ions M^{2+} (M = Mn, Cu, Zn) with the divacant $[\gamma\text{-SiW}_{10}O_{36}]^{8-}$. Therefore the reaction mechanism is complex since it involves insertion, isomerization, and dimerization as well as loss of tungsten. There is evidence that the structural type $[\{\beta\text{-SiM}_2W_{10}O_{36}(OH)_2(H_2O)\}_2]^{12-}$ which has been isolated for M = Ni^{2+} represents an intermediate for M = Mn^{2+}, Cu^{2+}, Zn^{2+} during the synthesis of **1**, **2**, and **3**.

It has been demonstrated that reaction of the metastable $[\gamma\text{-SiW}_{10}O_{36}]^{8-}$ with first-row transition metal ions can lead to polyoxoanions with unexpected structures and interesting magnetic properties. More work on this topic is in progress.

Supporting Information Available: Three X-ray crystallographic files, in CIF format. This material is available free of charge via the Internet at http://pubs.acs.org.

IC000078G